Fundamental investigation on the frost resistance of mortar with microencapsulated phase change materials

Romero Rodríguez, C.; França de Mendonça Filho, F.; Chaves Figueiredo, S.; Schlangen, E.; Šavija, B.

DOI
10.1016/j.cemconcomp.2020.103705

Publication date
2020

Document Version
Final published version

Published in
Cement and Concrete Composites

Citation (APA)
Romero Rodríguez, C., França de Mendonça Filho, F., Chaves Figueiredo, S., Schlangen, E., & Šavija, B. (2020). Fundamental investigation on the frost resistance of mortar with microencapsulated phase change materials. *Cement and Concrete Composites*, *113*, Article 103705. https://doi.org/10.1016/j.cemconcomp.2020.103705

Cement and Concrete Composites 113 (2020) 103705

Contents lists available at ScienceDirect

Cement and Concrete Composites

journal homepage: http://www.elsevier.com/locate/cemconcomp

Fundamental investigation on the frost resistance of mortar with microencapsulated phase change materials

C. Romero Rodríguez *, F. França de Mendonça Filho, S. Chaves Figueiredo, E. Schlangen, B. Šavija

Microlab, Department of Department of 3MD, Faculty of Civil Engineering and Geosciences, Delft University of Technology, Stevinweg 1, 2628CN, Delft, the Netherlands

ARTICLE INFO

Keywords:
Phase Change materials
Freeze/thaw cycles
Mortar
Microstructure
X-ray microtomography

ABSTRACT

Recent studies have shown that concrete containing Phase Change Materials (PCM) with low transition temperatures may reduce the number of freeze/thaw cycles suffered by the cementitious composite in temperate climates. Nevertheless, the positive influence of such admixtures on the frost resistance of cement-based materials has not been directly shown, nor the negative. In this study, mortars with different contents of microencapsulated PCM by volume of cement paste were studied with regard to the progression of their internal and salt scaling damages during freeze/thaw cycles. X-ray micro tomography was used to monitor damage development and spatial distribution in the mortars. Furthermore, the pore system and microstructure of the PCM-modified mortars were characterized to unveil the causes of the observed macroscopic behavior during frost weathering. The results show that limited amounts of PCM in mortar, namely 10 % by volume of cement paste, results beneficial for the frost and scaling resistance of the composite. Whereas, for larger PCM additions, like 30 % by volume of paste, the changes in microstructure, porosity and mechanical strength brought in by these admixtures resulted in worsened performance against freeze/thawing cycles.

1. Introduction

Concrete structures in cold climates may deteriorate due to frost action. Freezing and thawing cycles may cause significant damage to structures such as concrete pavements, retaining walls, and bridge decks [1]. At temperatures below 0 $^{\circ}C$ the pore solution of concrete will freeze [2]. As the volume of ice is larger than the volume of the pore water, it will cause expansive pressures in the concrete unless there is sufficient space to accommodate this expansion [3]. It has been also proven that as the ice lenses form in larger cavities, gel water migrates from gel pores due to osmotic pressure [4]. In any case, the freezing temperature and expansive pressures are dependent on the pore size, with lower temperatures needed for freezing of water in smaller pores and more pressure generated in these same pores [5]. Once the expansive pressures reach such a level that results in tensile stresses exceeding the tensile strength of concrete, cracking will occur [5]. Cracks in concrete present rapid pathways for ingress of deleterious species, such as moisture, CO_2, and chlorides. Once these aggressive substances reach the reinforcement, they will lead to corrosion initiation and the end of service life. This may cause heavy expenditures for repair and replacement of such structures already at the early stage of exploitation. Therefore, excessive cracking should be avoided especially in cold climates where freezing and thawing often go hand in hand with application of deicing salts.

Traditionally, air entrainment has been used to increase the freeze/thaw durability of concrete structures [6]. Through the use of air-entraining admixtures, a controlled volume of air bubbles is intentionally introduced in the concrete. This way, additional space is created to accommodate the ice growth [7]. However, air entrainment has a practical drawback: the process may be influenced by the temperature, cement chemistry, presence of SCMs, and on-site factors [3]. Therefore, it would be of great practical use if a more controllable alternative than air entrainment was available.

In recent years the use of phase change materials (PCMs) for reducing the number of freeze/thaw cycles in concrete structures has been proposed [8–10]. PCMs are combined (sensible and latent) thermal storage materials that can store and dissipate energy in the form of heat. These materials absorb and release heat when they change their state from solid to liquid and the other way around. It is expected that concrete incorporating properly designed and dosed phase change materials

* Corresponding author.
E-mail address: c.romerorodriguez@tudelft.nl (C. Romero Rodríguez).

https://doi.org/10.1016/j.cemconcomp.2020.103705
Received 1 October 2019; Received in revised form 12 May 2020; Accepted 4 June 2020
Available online 19 June 2020

will be able to remain warm longer, thereby reducing the number of freeze/thaw cycles undergone by the concrete and consequently the damage.

Phase change materials can be introduced into concrete through four procedures: (1) by embedding PCM filled pipes/panels into concrete [11,12]; (2) by impregnating PCM in lightweight aggregate particles which are then used in the concrete mix [13]; (3) by using micro-encapsulated PCMs directly in the mix; and (4) by impregnating the liquid PCMs directly on the concrete surface [14].

In previous researches [15,16] it was proven both experimentally and numerically that the presence of such PCM resulted in a delayed undercooling of the cementitious matrix and a shortening of the frost period during freeze/thaw cycles. It would follow then that the onset of ice formation in the cementitious matrix would be delayed during the phase change and that the frost damage would be mitigated because the undercooling exposure time is reduced, which has been demonstrated to be beneficial in terms of frost resistance [17]. In Ref. [18] the authors proposed a numerical model to predict the internal damage caused by frost and concluded that mortar containing 25 % of PCM by volume of cement paste presented lower progressive damage than its reference mortar. To the authors knowledge, the assessment of internal damage due to frost of PCM mortar and concrete has been only addressed in Ref. [19]. Unfortunatley, the authors themselves acknowledged that mass loss measurement is not a good method to quantify internal damage.

It has to be emphasized that, although incorporation of PCMs may reduce the number of freeze/thaw cycles, it also has an effect on physical and mechanical properties of concrete. Even though several studies have shown that properly designed concrete containing PCM will undergo a lower number of freezing/thawing cycles compared to reference concrete, this alone is not sufficient to prove its efficiency in reducing the associated damage. It is critical to focus on the damage and its development as a consequence of the freezing/thawing cycles, as well as the influence of PCM addition on the properties of cementitious composites that impact frost resistance. The aim of this study is, therefore, to test the effectiveness of addition of microencapsulated phase change material (PCM) to cementitious materials in delaying the onset of damage caused by freezing/thawing cycles.

In the current study the influence of different PCM dosages on the resistance of mortar to internal damage and salt scaling during freeze/thaw weathering was studied. In order to explain the observed behavior, the hydrates assemblage, pore structure, coefficient of thermal expansion and mechanical properties of the studied composites were assessed. To evaluate the frost resistance of the mortars, standard methods such as relative length change and mass scaling were used. In addition, the samples damage was monitored through X-ray microtomography throughout the weathering regime after 1, 3, 7 and 14 cycles and the spatial distribution of the damage could be evaluated. The findings of this study provide a step towards practical implementation of PCM microcapsules for reducing freeze/thaw damage in concrete.

2. Experimental methodology

2.1. Materials and mixtures

Mortar samples were produced using CEM I 42.5 N (ENCI, Netherlands), tap water, Master Glenium 51 (BASF), quartz sand (Normensand) and encapsulated phase change material (Encapsys). The cement had a Blaine fineness of 295 m^2/kg. The superplasticizer, Master Glenium 51, had a concentration of 35 %. The quartz sand was standard with the size 0.08/2 mm. Fig. 1 shows the particle size distribution of the cement, phase change material and the sand. The chemical composition of the cement can be seen in Table 1.

The PCM used in this study consisted of paraffinic wax, encapsulated with melamineformaldehyde shells. Their latent heat of fusion of 131.27 J/g was obtained from heat flow measurements via differential

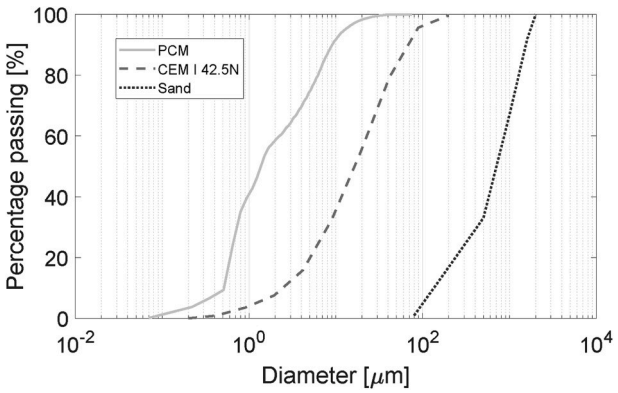

Fig. 1. Particle size distribution of raw particulate materials.

scanning calorimetry (DSC), using a DSC 8500 from PerkinElmer. The raw PCM were heated and cooled between −20 °C and 100 °C at a rate of 5 °C/min. The curves are shown in Fig. 2. During cooling the PCM presented two transition temperatures: one small peak at −6°C and a bigger one at −16°C whereas during heating the transition temperature was found to be 4°C. These admixtures thus, are likely to produce a supercooling effect in the pore solution of cementitious materials.

Three mortar mixtures with water-to-cement ratio of 0.5 were studied. These mortars contained PCM in different amounts: 0, 10 and 30 % by volume of cement paste. The cement paste content was kept constant for all the mixtures whereas part of the sand was replaced with PCM microcapsules. In order to prevent the presence of air voids in the mortar samples, the superplasticizer content of each mixture was adjusted to obtain a flow table test diameter of 185 *mm*. The resulting mix designs of the mortar mixtures are shown in Table 2.

A Hobart planetary mixer was used to prepare the fresh mortar. All dry components were mixed first for 1 min at low speed. Previously mixed water and superplasticizer were added into the running mixer in the following 30 s and the components were left to mix for extra 30 s. Afterwards, the walls of the mixer were scraped and the mixture was left to mix for 1 min and 30 s at low speed and 30 s at medium speed. Casting of the fresh mortar was carried out in two layers followed each time by 15 s in the vibrating table. The samples were then sealed and left to harden for 24 h in laboratory conditions. Afterwards the samples were demoulded and stored in a fog chamber with temperature and relative humidity set as 20°C and 95 %, respectively until the age of testing.

2.2. Characterization methods

2.2.1. MIP and gravimetric method

Mercury Intrusion Porosimetry (MIP) was performed by means of a Micrometrics PoreSizer 9500. Maximum pressure of the device was 210 *MPa*, which corresponds to a minimum pore diameter of 7 *nm* using a cylindrical pore model.

Using the aforementioned cylindric pore model, the diameter of intruded pores, D, can be calculated using Washburn's equation [20]:

$$D = \frac{-4\gamma \cos\theta}{P} \quad (1)$$

where γ is the surface tension of mercury (0.485 N/m at 25° C), θ is the contact angle between mercury and mortar, taken as 139 ° for intrusion and 106 ° for extrusion, and P is the applied pressure.

Thin slices of 3 *mm* thickness were sawn from 90 days old samples for mercury intrusion porosimetry (MIP) measurements. In order to stop hydration and dry the slices solvent exchange with isopropanol was used. In a first moment the slices were subjected to five short periods of alternated immersion in the solvent and drying in air to stimulate fast absorption. Afterwards, the samples were left immersed for 7 days to ensure complete exchange [21]. To accelerate the evaporation of

Table 1
Chemical composition of CEM I 42.5 N in [%].

CaO	SiO_2	Fe_2O_3	Al_2O_3	SO_3	MgO	K_2O	TiO_2	P_2O_5	Rest	Loss on ignition
69.53	15.6	3.84	3.09	2.6	1.67	0.55	0.31	0.14	0.53	2.14

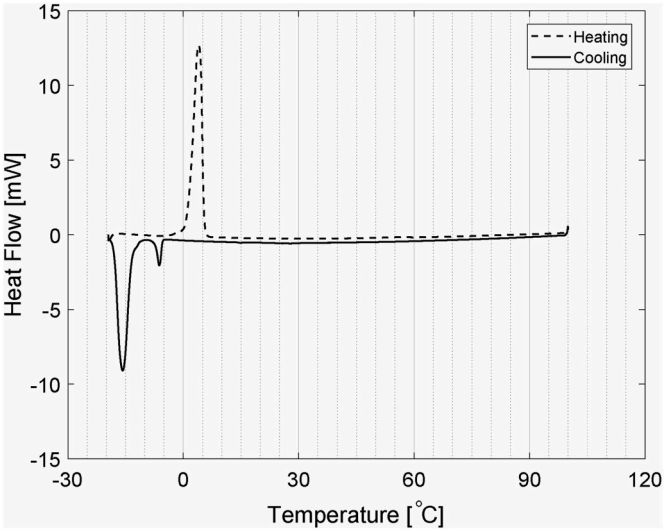

(a)

Fig. 2. Differential scanning calorimetry of EnFinit powder PCM.

Table 2
Mix design of mortars.

Components	Weight [kg/m^3]		
	REF	PCM10	PCM30
CEM I 42.5 N	514.1	514.1	514.1
PCM	0	38.6	115.7
Water	257	257	257
Superplasticizer	0.22	0.44	1
Total aggregates	1542.2	1428.2	1200.3
1.6-2 mm	200.5	185.7	156.0
1.28-1.6 mm	308.4	285.6	240.1
0.5-1.28 mm	524.4	485.6	408.1
0.16-0.5 mm	385.6	357.1	300.1
0.08-0.16 mm	123.4	114.3	96.0

isopropanol the slices were vacuum dried for 1 h and put in a desiccator until testing. The slices were carefully cut into regularly shaped pieces of 5 mm size prior to the test. For each test around 6 pieces were used for a total mass of 3.5 g. For each mortar, three tests were performed.

Gravimetry was also employed to assess the porosity accessible to water of mortar cylinders.

($\varphi = 35$ mm and height of 70 mm) via the following formulation:

$$p = \frac{m_{sat} - m_{dry}}{m_{sat} - m_{imm}} \quad (2)$$

where m_{sat} is the mass of the sample after water saturation under vacuum for 24 h, m_{dry} is the mass after drying till constant weight attainment in an oven at 105°C and m_{imm} is the hydrostatic weight of the sample. Three samples were used per mortar mixture.

2.2.2. Scanning Electron Microscopy and image analysis

Scanning Electron Microscopy (SEM) in Back Scattered Electrons (BSE) mode was performed on the different studied mortars in order to investigate the influence of PCM addition on the hydrates assemblage in the cementitious matrix.

At the age of 90 days, 40 × 40 × 160 mm prisms, made out of mortars REF, PCM10 and PCM30 and previously dried in an oven at 40°C degrees, were sawn into 10 mm thick transversal slices. The slices were further cut into pieces of side 1.2 cm, from which only the piece at the core was further prepared for microscopy. At this point the selected slices were impregnated with epoxy resin and later ground at 150 RPM with 1200 grade Silicon Carbide paper and using ethanol as lubricant until discovering of the mortar surface, for about 1 min. Following grinding, the slices were put in an ultrasonic bath while immersed in ethanol and successively rinsed. They were then polished using 6, 3 and 1 μm diamond pastes from Struers for 15, 15 and 30 min with intermediate immersion and rinsing as described previously. The polished slices were kept in a desiccator until testing time and a 10 nm carbon coating layer was applied just prior to the microscopy.

An Environmental Scanning Electron Microscope (ESEM XL30, FEI, Thermo Fisher Scientific) was used at high vacuum for the acquisition of the micrographs. The instrument was operated with accelerating voltage of 15 kV and at a distance between condenser lense and specimen surface of 10 mm, with a magnification of 500×. From each mortar 30 BSE images were acquired from regions without aggregates or with only small portions of aggregates at the boundaries. The resulting field of view was 252 × 189 μm^2.

The obtained 16-bit BSE images were then segmented using the plugin from ImageJ [22], Trainable Weka Segmentation (TWS) [23] to distinguish between anhydrous phases, portlandite, low and high density CSH, pores/PCM macropores and aggregate portions.

2.2.3. Coefficient of thermal expansion

The coefficient of thermal expansion of the studied mortars was measured in 90 days old beams with dimensions 160 × 40 × 40 mm. For each mortar mixture, three samples were used for the measurements. The samples were dried in the oven at 40°C until constant mass attainment and afterwards wrapped with self-adhesive aluminium tape and put back in the oven to promote an even moisture distribution inside the samples.

Given the difference in heat capacity of the samples at subzero temperatures due to the presence of the PCM, it was decided to measure the thermal expansion on a range of positive temperatures. The samples were subjected to a series of isothermal steps in an environmental chamber at 40% relative humidity. A thermocouple was inserted in one of the samples to monitor the sample internal temperature versus the temperature set in the chamber. The temperature steps were set as 10, 20, 30, 40 and 50°C. The length change in the samples was measured by means of linear variable differential transducers (LVDT) placed on two parallel faces of the prism along the span via glued invar holders. The scheme is shown in Fig. 3. The measurements on 3 mortar specimens were calibrated with the measurements on a quartz specimen with identical LVDTs configuration.

2.2.4. Mechanical properties

Three mortar prisms (160 × 40 × 40 mm) per mixture were tested in three point bending (3 PB) configuration at the age of 28 days. The halves of the prisms were used to test compressive strength of the mortar on cubes of 40 mm side. A servo-hydraulic mechanical press with maximum load capacity of 5000 kN and high stability from Matest was employed. The rate of loading was fixed at 13.5 kN/s for compression testing and 0.5 kN/s for flexural testing, respectively.

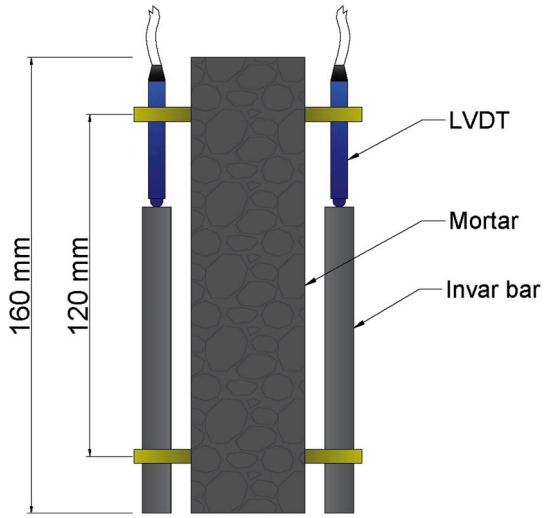

Fig. 3. Scheme of LVDTs configuration for the measurement of the coefficient of thermal expansion (dimensions in *mm*).

2.3. Freeze and thawing weathering and monitoring

2.3.1. Freeze and thaw cycles

The studied mortars aged 28 days were subjected to 7 cycles of freezing and thawing with de-icing salts. Two types of samples were exposed to the weathering conditions: prims and cylinders, the dimensions of which are described in the following sections. The samples were taken out of the curing chamber and immediately exposed to the freezing medium for 24 h prior to the first cycle. The freezing medium consisted of a NaCl solution with 3 % concentration. Each cycle consisted of 16 h of exposure at $-21^{\circ}C$ and 8 h at $21^{\circ}C$ in a freezing cabinet and at standard laboratory conditions, respectively. Such cycle settings were chosen in order to accelerate the damage in the samples rather than to simulate realistic frost exposure of concrete elements [17]. It is reported that the longer the time during which the minimum cycle temperature is kept, the higher the obtained internal damage [24,25], which in turns will accelerate scaling damage. PCM are expected then to reduce this exposure time by delaying the onset of ice formation due to the release of heat at $-6^{\circ}C$ and $-16^{\circ}C$ when phase change occurs. Furthermore, also the temperature gradient in the sample is expected to decrease with the presence of PCM additions.

During exposure all samples were thermically insulated by means of styrofoam, except for the bottom 3 *mm* which were left exposed to the freezing medium set equally high in the samples container. A scheme of the configuration is shown in Fig. 4.

2.3.2. Relative length change and mass scaling

Three mortar prisms per mortar with dimensions $160\times 40\times 40$ *mm* and cast-in steel inserts were used for the measurement of frost salt scaling and relative length change after 1, 3 and 7 freeze–thaw cycles.

The mass scaling was measured following the recommendations in Ref. [26]. The samples were first sprayed with demineralized water and the debris collected in filter paper, then a brush was used to gently scrape off the scaled surface followed by further spraying and collection of later debris in the same filter paper. The scaled material was allowed to dry in an oven set at $105^{\circ}C$ until constant mass attainment.

The length change along the span of the beams was then measured by means of a length comparator to the nearest 0.001 *mm*. For each measurement the length of a reference invar rod was first tared and then the length difference between it and the mortar sample was recorded. The steel inserts, placed in the centre of the bases of the prisms, allowed the measurement of the specimen length between the exact same spots every time. Furthermore, two invar steel spheres were put between the steel inserts and the length comparator contacts.

2.3.3. X-ray micro computerized tomography (μCT)

The progressive damage resulting from frost action was monitored through X-ray microtomography after 1, 3,7 and 14 freeze/thaw cycles. Measurements were performed on mortar cylinders with a height of 40 mm and a 21 mm diameter. For the imaging, only one sample per mortar was monitored.

The samples were scanned using a Micro CT-Scanner (Phoenix Nanotom, GE, Germany). The X-ray tube was operated at 140 kV and 160 μA. Some 1441 projections were acquired by a digital GE DXR detector (2288×2304 pixels). Each projection was the resulting average of 4 radiographs with an exposure of 500 ms in order to minimize noise. The voxel resolution under these conditions was 11 μm.

After calibrating the projections with dark and bright field images, 3D reconstruction of the acquired projections was performed using the software Phoenix datos|x Reconstruction 2.0. During the reconstruction, ring, spot and beam hardening artifacts were corrected. With the opensource software DataViewer (Bruker), the reconstructed scans from different weathering time points were registered to study progressive damage in the individual samples. This allowed for the spatial correspondence of different scans from different time points. Image analysis was then performed using the freeware ImageJ [22].

3. Results

3.1. Physical and mechanical properties of mortar with PCM

3.1.1. Hydrates assemblage

In Fig. 5 representative Grey Value scale (GV) micrographs, acquired for the studied mortars, are shown. In this figure, also their corresponding segmentations in Red Green Blue scale (RGB) are reported. Some differences can be spotted from mere observation, such as the increasing presence of spherical PCM macropores from PCM10 to PCM30. From the segmented micrographs quantitative analysis was undergone. In a study from Scrivener [27], the author discussed some limitations of quantitative analysis through 2D microscopy nevertheless, the technique still remains a fair tool for quantitative comparison.

The degree of hydration, α, of each mortar matrix was calculated as average of the values computed for each micrograph according to the ratio proposed by Powers and Brownyard [28] in which the authors assume that hydration products occupy a volume 2.1 times larger than

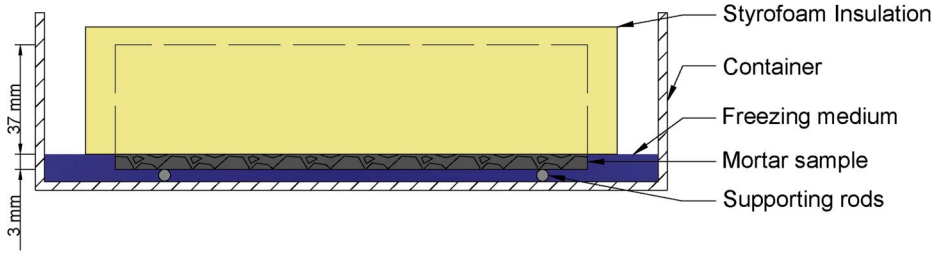

Fig. 4. Scheme of the freeze/thaw weathering setup for mortar beams.

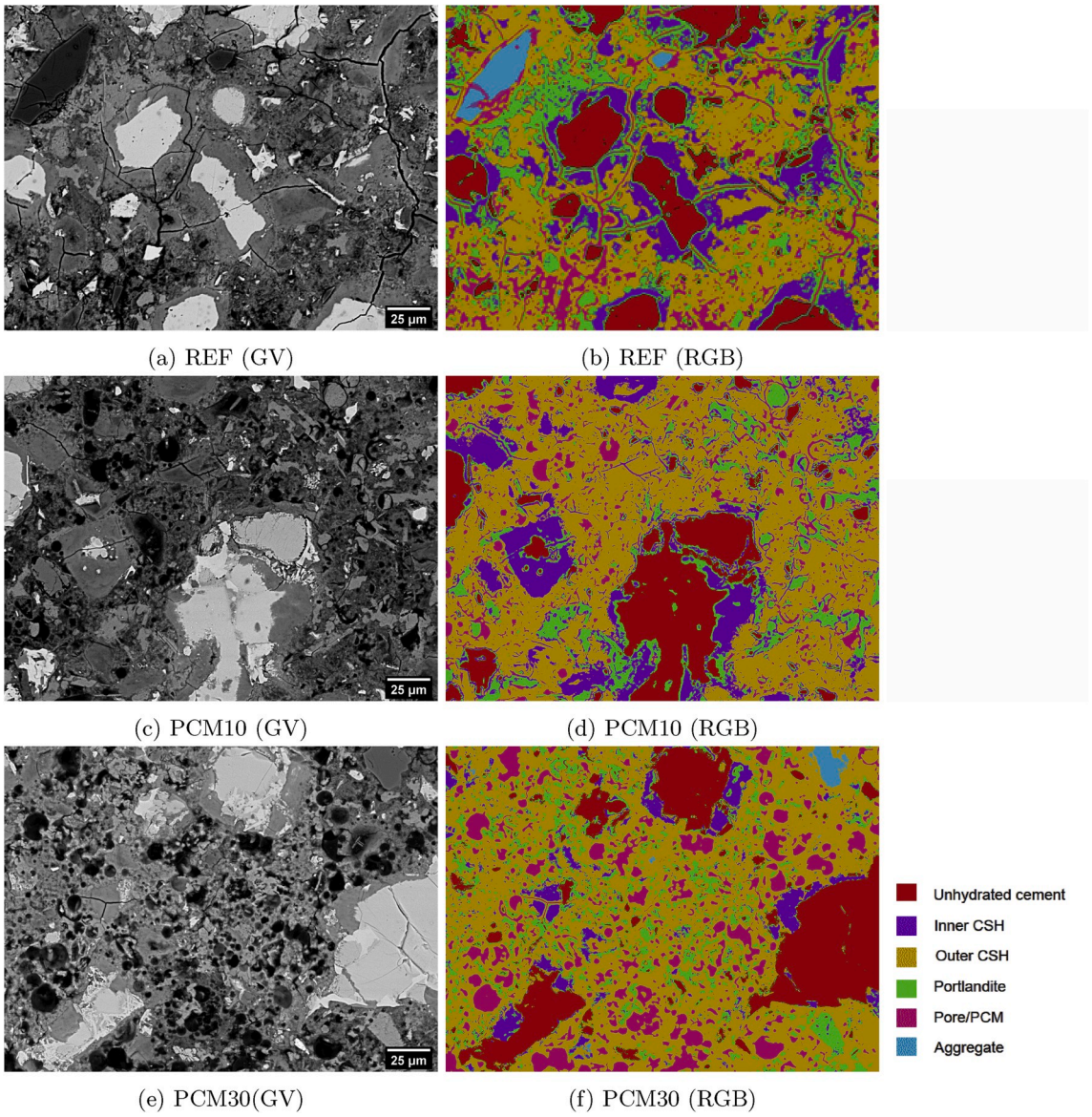

Fig. 5. Grey Value scale (GV) micrographs of REF a), PCM10 c) and PCM30 e mortar and their segmentations in Red Green Blue (RGB) scale through Weka segmentation plugin in b),d) and f), respectively. (For interpretation of the references to colour in this figure legend, the reader is referred to the Web version of this article.)

their originating unhydrated cement particles:

$$\alpha = \frac{F_{hp}/2.1}{F_{hp}/2.1 + F_{uc}} \tag{3}$$

where F_{hp} and F_{uc} are the volumetric fractions of hydration products and unhydrated cement.

Hydration degree values of 90 days old mortars were 0.68, 0.74 and 0.73 for REF, PCM10 and PCM30, respectively. Although it has been shown that the degree of hydration via SEM analysis is slightly underestimated [29], the values can be used to compare between the reference mortar and both mortars containing PCM. In this regard, PCM might have influenced the kinetics of cement hydration to an extent when comparing PCM mortars to the reference. Nevertheless almost no difference was found between the two PCM mortars studied.

In Fig. 6 the estimated fractions of main hydration products (Portlandite, low density and high density CSH) are summarized. From these results it can be observed that Portlandite content slightly decreased from 0.18 to 0.15 and 0.16 with the addition of 10 and 30 % of PCM by volume of cement paste, respectively. Nonetheless, the average values do not seem to follow a trend when varying the PCM dosage. In fact, CH content of PCM30 is higher than that of PCM10, which may even indicate a variation within the results own deviation. In any case, this finding was unexpected since in a previous study [30] the authors suggest that PCM particles acted as nucleation sites for the hydration products. Nevertheless, the PCM microcapsules employed in the present study presented a d_{50} of about 12 μm, slightly different from those employed by the authors in Ref. [30] of 7 and 10 μm. Furthermore, the PCM used in the aforementioned study had a transition temperature peak during heating at around 24 $^{\circ}C$ which may have affected the heating rate of mortar during early age hydration. It has been shown before that temperature rate has influence on nucleation and growth of crystals [31].

Regarding inner CSH content, a 37 % reduction was observed in PCM30 when compared to the fractions measured for the reference mortar. On the other hand, the fraction of inner CSH for PCM10 was comparable to the reference.

Opposite to the trend observed for inner CSH fractions, the outer CSH

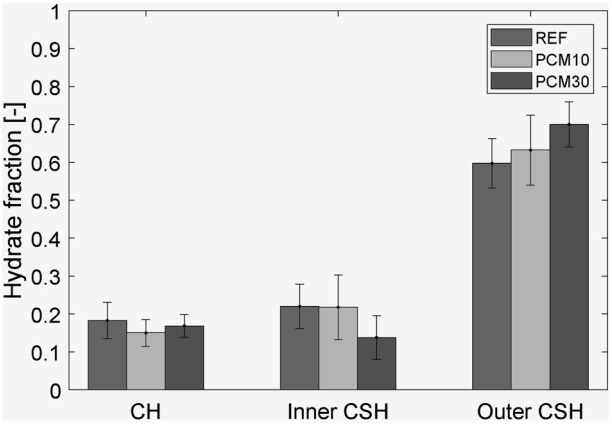

Fig. 6. Volumetric fractions of portlandite (CH), high density CSH (inner CSH) and low density CSH (outer CSH) in the studied mortars.

content seemed to increase consistently with the increase of PCM dosage up to 17 % with respect to the reference mortar.

These results confirm that the presence of PCM in cementitious matrix modifies the microstucture of the composites. In a study from Ref. [32], the authors proved that the melamine formaldehyde (MF) shell potentially degrades and partially breaks in cementitious matrices due to hydrolysis in sulfate-bearing environments, especially at early stages. In such conditions the paraffinic wax contained in the microcapsules might partially migrate and somehow interfere the hydration reactions. In light of the observations presented herein, this effect would probably be more pronounced for composites with higher PCM percentages (PCM 30) and thus be (at least partly) responsible for the reduction in high density CSH content.

3.1.2. Pore structure

The porosity accessible to water of the studied mortars does not provide a pore size distribution but the total open porosity including micro, meso and macro pores. The values for REF, PCM10 and PCM30 were found to be 17.7 %, 20.5 % and 24 %, respectively. Mortar REF presents the lowest volume of open porosity. PCM30 shows a relevant increase in porosity of around 35 % with respect to the reference mortar. These values were used as input to determine the amounts of material used for MIP measurements.

Fig. 7 shows the cumulative pore size distributions and the differential intruded volume of REF, PCM10 and PCM30.

The cumulative pore volume from MIP seems to follow the same trend as from the gravimetric results. The values for REF, PCM10 and PCM30 were found to be 14.1 %, 15.3 % and 18.7 %, respectively. When more PCM are added to the mortar the total porosity also increases. Such increment in cumulative porosity was very smal for PCM10 when compared to the reference mortar but became substantial for PCM30. From the cumulative porosity curves it was also possible to observe that for PCM mortars the ink-bottle porosity rose and therefore the porosity effective for transport processes was reduced when PCM are added. More specifically the effective porosity resulted 6.6, 5.4 and 6.1 % for REF, PCM10 and PCM30, respectively.

From the pore size distribution it could be observed that there is a reduction of the critical pore diameter when PCM were added in the mortars. Moreover, the magnitude of the later decrement seems to decrease for increasing addition of PCM with respect to the critical pore diameter of the reference mortar. In Ref. [30] the authors MIP results also suggested a decline in the critical pore diameter until a PCM replacement level of 15 % of cement paste volume. Afterwards, the critical pore diameter increased albeit remaining below the reference mortar corresponding value. In the present study, it was also possible to notice that the increase of PCM amount resulted in larger pore volume in the range between 10 and 20 nm size, as seen from the shoulders in the differential pore volume curves of both PCM10 and PCM30, which may correspond to an increase in gel porosity [33]. These results are confirmed by what has been discussed in Section 3.1.1, from BSE analysis, where it was shown that higher amounts of PCM in the mortar result in a steady increment of the outer CSH fraction and/or a decline of the fraction of inner CSH. Another yet important observation is that while a small amount of PCM resulted in a clear refinement of the pore structure, for higher replacements of aggregates by PCM, the capillary porosity became dominant when it came to mercury percolation, in addition to the boosted gel porosity.

These results seem to indicate that whereas the inclusion of small amounts of PCM in mortar leads to refined pore structure, replacement of sand volume by a higher volume of PCM microcapsules increases also the capillary porosity of the mortar in addition to the gel pores. In this regard it is believed by the authors that the replacement might have come with an increase of specific surface area of the interface between cement paste and aggregate/PCM.

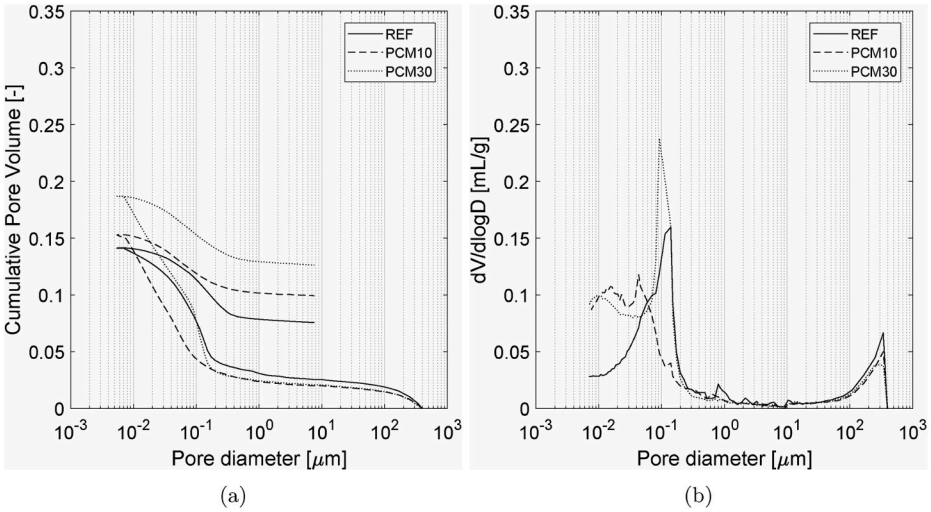

Fig. 7. Pore size distribution of mortars REF, PCM10 and PCM30 represented as a) cumulative (during intrusion and extrusion) and b) differential (curing intrusion only) pore size distribution.

3.1.3. Coefficient of thermal expansion

The thermal dilations of the studied mortars are reported in Fig. 8 for a range of temperatures from 9° C to 48° C. The thermal expansion coefficient (TEC) was obtained by means of linear regression. For each mixture 3 samples were tested and a total of 6 measurements were obtained from the LVDTs reading. In Fig. 8, the average and the standard deviations are also plotted. The resulting TEC were 12.08 ± 0.61, 13.28 ± 0.65 and 16.24 ± 0.83 $\mu m/m$ for REF, PCM10 and PCM30, respectively. The thermal dilation of the samples was found to increase when a larger volume of aggregates was replaced with the PCM. The presence of standard quartz aggregates in cementitious materials has been shown to decrease the TEC of the overall composite [34], due to the lower TEC of mortars when compared to cement pastes. It seems that PCM microcapsules do not provide the same effect, probably due to their much smaller dimensions, lower stiffness and thermal stability.

3.1.4. Mechanical properties

The average compressive and flexural strengths of mortars REF, PCM10 and PCM30 are shown in Fig. 9. The inclusion of 10 and 30 % of PCM by volume of cement paste results in a decrease of the compressive strength by 35 and 55 %, respectively. The decrease in flexural strength was less pronounced with 23 and 32 % for PCM10 and PCM30. Since a fraction of the quartz aggregates were substituted with soft inclusions, the replacement of a material with high mechanical strength by one with little mechanical resistance could be a possible explanation for the observed loss in strength. The alleged effect of increased heterogeneous nucleation of cement hydrates due to the increase in surface area by the PCM was found to be negligible at high aggregates replacement levels in Ref. [35]. The authors explained that the absence of hard inclusions was far more deleterious. In a study from Chen et al. [36], the authors proposed an empirical relationship between porosity (p) and compressive (f_c)/flexural strength (f_{fl}). The latter were based on data obtained from tests on 28 days old mortars samples with same dimensions and type of cement as in this study. These predicting relationships were here used to understand if the sole substitution of aggregates with soft inclusions (PCM) can be responsible for the loss of mechanical strength in the mortar. First, if the PCM are considered as additional pores (strength--wise) to the reference mortar, the mechanical porosity results to be 0.21 and 0.3 for PCM10 and PCM30, respectively. Such increases in porosity would result in predicted decrements of compressive strength of 14 and 38% for PCM10 and PCM30, respectively. Regarding flexural strength, predicted decreases would be of 10 and 21%, respectively. When the predicted losses of strength are compared to the ones measured for PCM10, there are 21 and 13% of compressive and flexural strength loss, respectively, unaccounted for. In the case of PCM30 the discrepancy between predicted and measured compressive and flexural strength losses are 17 and 12 %, respectively. Next, when the increase in capillary and gel porosity in PCM10 and PCM30, measured from gravimetry and MIP as in Section 3.1.2, are taken into account, the predictions for PCM10 are still 11% short of compressive strength loss and 6% of flexural strength decrement. Whereas in the case of PCM30 the predicted losses fall closer to the measured ones by 0 and 3% for compressive and flexural strength, respectively. These analyses suggest that although the substitution of aggregates with weaker PCM contributes considerably to the decrease of compressive and flexural strength, the increase on capillary and gel porosity equally impacts such properties. Furthermore, there are additional losses of strength that cannot not be attributed only to the aforementioned causes, especially for lower aggregates replacement levels (PCM10).

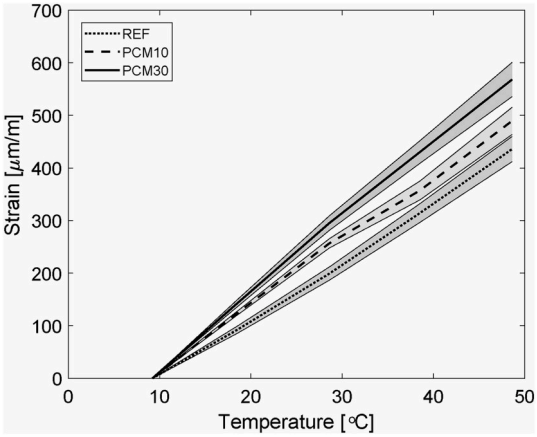

Fig. 8. Measured thermal dilations in studied mortars REF, PCM10 and PCM30.

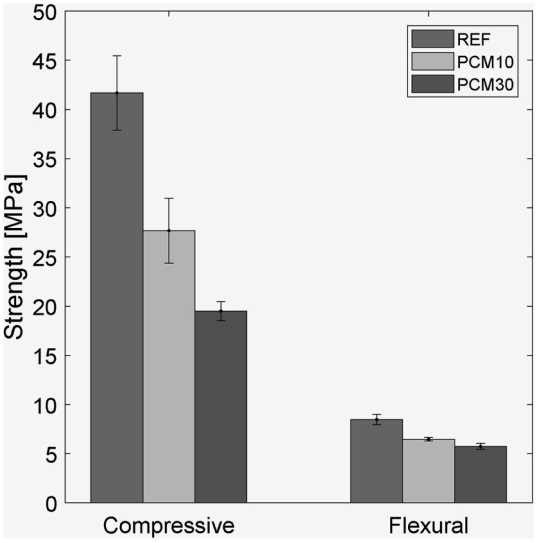

Fig. 9. Compressive and flexural strength of the studied mortars REF, PCM10 and PCM30.

In a study by Falzone et al. [37] it is suggested that the ITZ associated with the PCM significantly reduces the composite stiffness. Alternatively, the loss of strength was attributed to capsule breakage during mixing and the resulting interaction of leaked PCM and cement during hydration in Ref. [38]. This interaction could modify the hydration products and/or result in increased porosity. Other research [30,39] has shown that the breakage of the capsules results in the agglomeration of PCM from multiple capsules which may introduce numerous weak zones. Another likely cause for the large strength drop for PCM30 samples is the lower volume of inner CSH for a high level of PCM dosage such as 30 % by volume of cement paste as it has been shown in Section 3.1.1. In other studies [40,41] it has been experimentally determined that inner and outer CSH present diverse micromechanical properties with the earlier possessing higher elastic modulus and tensile strength.

3.2. Frost damage of mortar with PCM subjected to freeze and thaw cycles

3.2.1. Length change and mass scaling

The relative length change of the samples along the central line, measured after 1, 3 and 7 cycles of freezing and thawing is shown in Fig. 10a in logarithmic scale. No significant differences between the different mortars were observed after cycle 1, apart from the high variability in length change for mortar PCM10. The change in length for REF and PCM10 remained similar after the third cycle at 0.0112 and 0.0136 %, respectively. The change in length for PCM30 samples was 0.394 %, one order of magnitude higher. After 7 cycles, the change in length of PCM10 negligible at 0.0142 %, whereas REF samples length increased to 0.0272 %. PCM30 exhibited a length change two orders of magnitude higher than the other two mortars at 1.065 %. At the

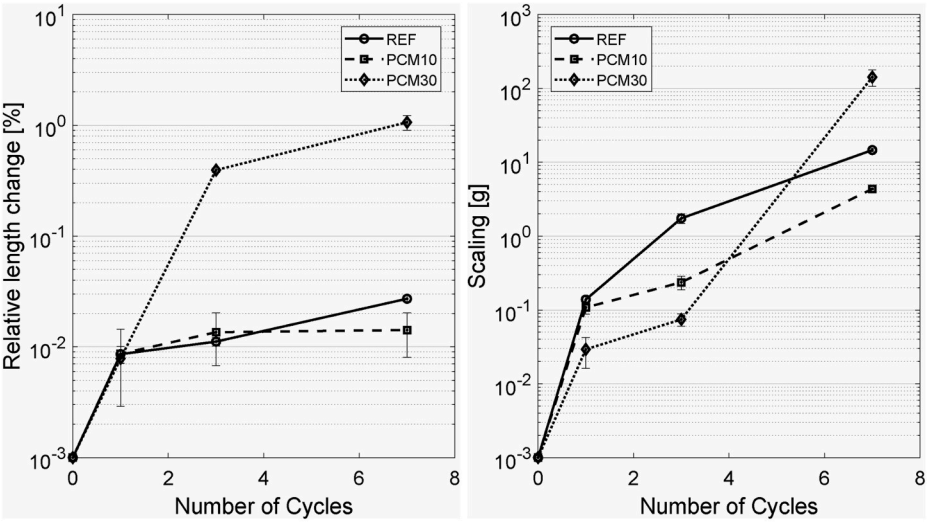

Fig. 10. Relative length change a) and mass scaling b) of mortars REF, PCM10 and PCM30 during freeze/thaw cycles.

completion of the tests, the highest degree of damage was observed for the mortar with 30 % of PCM by volume of cement paste, followed by the reference mortar. It can therefore be concluded that 10 % of PCM in mortar will generate the least internal damage.

The progressive mass scaling of the studied mortars are shown in Fig. 10b. Mass scaling was observed for all materials after one cycle as expected, given the harsh weathering conditions. The trend was as follows. The least damage was observed for PCM30 with only 0.03 *g*. Whereas the control mortar and PCM10 presented markedly more scaling at 0.14 and 0.11 *g*. The same fashion was obtained after the 3 cycles. Only after 7 cycles PCM30 overtook the reference and PCM10 mortars, exhbiting a mass scaling of 142 *g*. The magnitude of deterioration of PCM30 was one order of magnitude higher than the other mortars. Visually, the part of the PCM30 samples protruding from the insulation was completely eroded after collection of the scaled debris.

When comparing both types of frost damage, internal and scaling, as measured through relative length change and mass scaling, the same end result is obtained after 7 cycles. It is suggested from these measurements that an addition of 30 % of PCM on the mortar yielded a marked worsening of the internal damage and scaling with respect to the reference mortar. Whereas an addition of only 10 % of PCM resulted in improved resistance to freezing and thawing cycles. Nonetheless, there seems to be a delay on the scaling damage of PCM30 which presented signs of abnormally increased relative length change after 3 cycles while the marked scaling was only relevant afterwards. Whether these two damage types are caused by the same or different mechanisms cannot be said from the mere ocurrence of both damages with the same trend [17]. Nevertheless it might be an indication that the same material risk factors influence the mechanism(s).

3.2.2. *Progressive damage monitored through X-ray micro tomography*

In Fig. 11, we show progressive damage in the same region of interest (ROI) for each sample in REF, PCM10 and PCM30 after 0, 1, 3, 7 and 14 weathering cycles. The three ROI's were located near the edges where the scaling occurred and because there were more visible cracks. Most likely cracks close to the edges appeared wider because expansion is possible there. Else, the quantification and identification of internal microcracks were only possible from differential tomography as will be seen later in this section.

It is worth noticing that from the GV images it is hardly possible to distinguish aggregates from paste for the REF sample. As the amount of PCM in the mortar is increased, the contrast becomes more evident, as seen in the slices from PCM10, but especially for those from PCM30. This is due to the drop in density caused by the addition of PCM microcapsules. It is known that X-ray attenuation is dependent on the density of the material, as well as on the beam intensity and thickness of the penetrated material according to the Beer–Lambert law [42,43]. Moreover, it was shown in sections 3.1.1 and 3.1.2, that the addition of these admixtures resulted in increased outer CSH fraction and hence gel porosity. In section 3.1.4, it is especulated that the increase of low density CSH gel and porosity contributes to the drop in mechanical properties since the micromechanical ones are probably weakened. In that regard it has been proven in Ref. [44] that there exists a correlation between GV from X-ray microtomography and microhardness and Young's modulus of cementitious materials.

Another clear difference between the studied samples is the increasing presence of air voids for higher dosages of PCM in the mortars despite the use of superplasticizer to compensate for the worsening of the workability.

It is obviously not possible to generalize from one single ROI per studied mortar, hence from these 2D slices general considerations were made regarding the propagation of damage due to frost action for the boundary conditions used in the experiments herein. Cracks, both near the edge or in the core propagated mainly through the interface transition zone (ITZ). Sparingly, cracks also propagated through the aggregates like it can be seen in the slice shown in Fig. 11i, l and 11o. It was common to observe pre-existing microcracks progress throughout the weathering regime. In 11b, 11e, 11h, 11k and 11n, example of such cases is reported in the upper region of the ROI. Another common damage cause was the crack nucleation and propagation from existent of macrodefects near the edges at the exposed surface. An instance of such cases is reported in Fig. 11a, d, 11g, 11j and 11m. It can be followed by means of the X-ray microtomography that a crack propagated radially from the defect in 11d, followed by deformation of the tip of the macropore after 3 cycles in 11 g, crack enlargement in 11j and eventual chipping (11 m).

The reconstructed scans after 1, 3, 7 and 14 cyles were substracted from the initial one at 0 cycles. From these differential micro tomograpghy's the volume of cracks and chips of material were quantified per slice. In this way a spatial distribution of the damage was obtained. In Fig. 12a, c and 12e vertical profiles of the damaged volume per slice are shown. The standardized height of the samples was used to account for the slight differences in absolute height among the studied samples. The damaged samples are shown in Fig. 12b, d and 12f after 14 cycles.

Foremost, after 3 cycles of freeze/thaw negligible damage was observed for REF and PCM10. In contrast by this time, PCM30 already

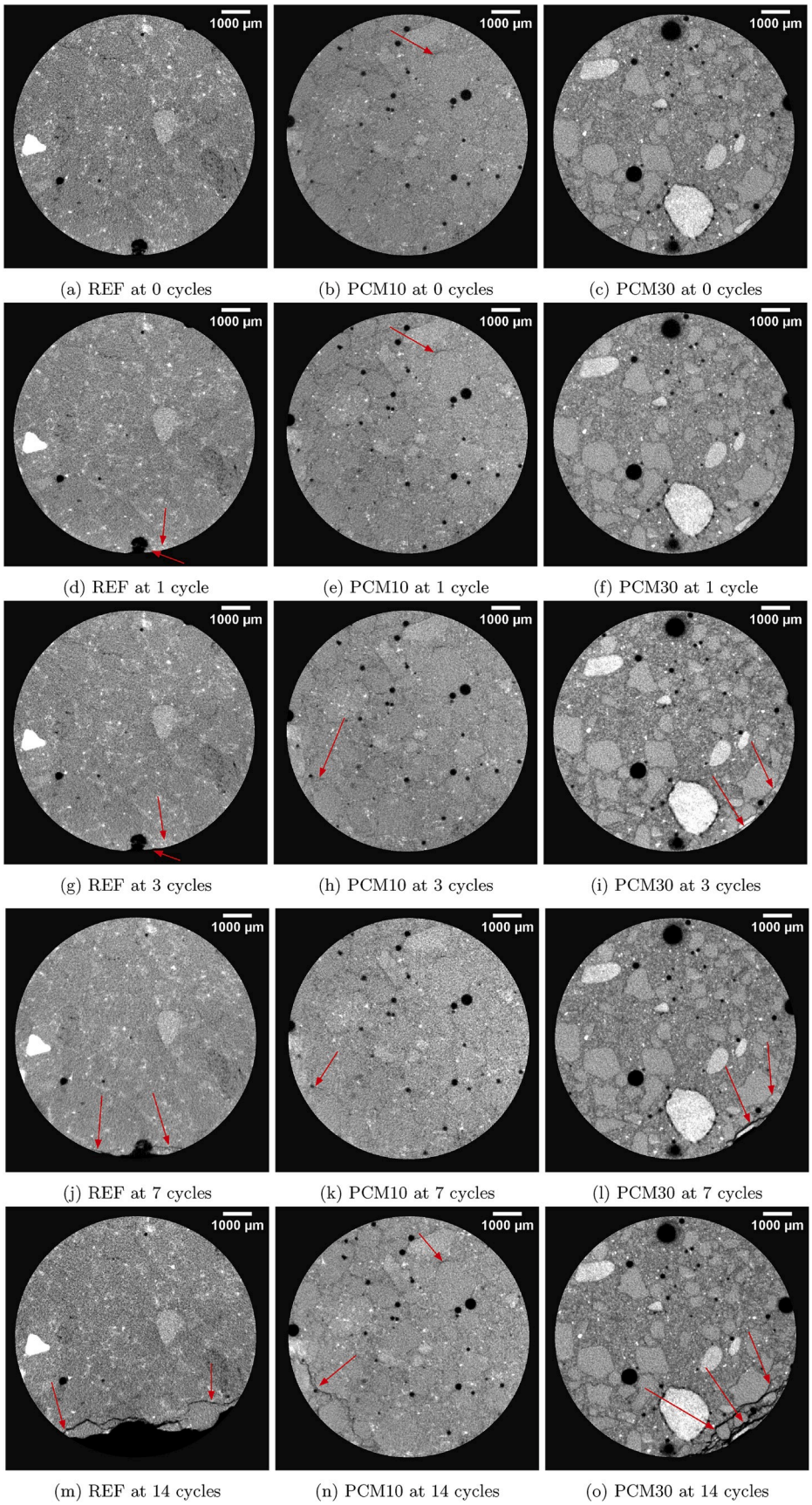

Fig. 11. 2D X-ray tomography slices of progressive frost damage in mortar samples after 0, 1, 3, 7 and 14 weathering cycles.

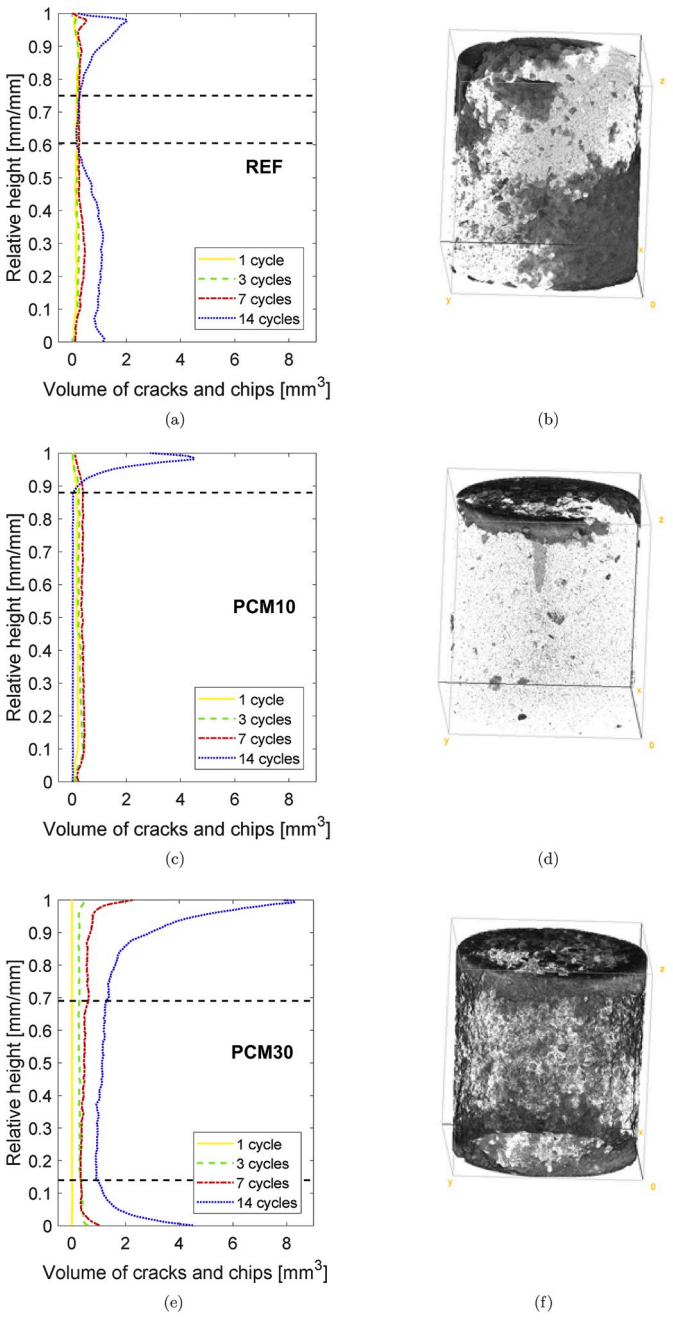

Fig. 12. Vertical distribution of frost damage after 1, 3, 7 and 14 freeze/thaw cycles for REF a), PCM10 c) and PCM30 e) quantified from X-ray micro tomography and renderization of the damage after 14 days (b, d and f).

displayed shallow chipping at the edges. After 7 cycles, increasing scaling damage become apparent for REF and PCM30. REF displayed some damage at 5 % of the height from the surface exposed to the freezing medium. PCM30 displayed damage at 14 % from the weathered surface and 4 % from the insulated one. In contrast PCM10 did not present any sign of damage due the weathering cycles. All studied samples had been affected after 14 cycles of freeze/thaw. Due to the size effect, critical frost damage of the cylindrical samples was observed 7 cycles later relative to that of the beams in Section 3.2.1. For REF, PCM10 and PCM30, the depth affected by frost salt scaling was measured at 25, 12 and 31 % of the height from the exposed surface, respectively. At 60 and 13 % from the insulated surface, the reference mortar and the mortar with 30 % PCM also displayed damage, albeit lower in degree than the damage near the weathered surface.

4. Discussion

The introduction of PCM admixtures with low range of transition temperatures had indeed a relevant impact on the frost resistance of mortar as evinced from the results presented in the previous section.

PCM10 presented a markedly better performance against frost salt scaling action when compared to the reference mortar and a small improvement is inferred from the length change measurement and hence also a reduction of the internal damage due to frost. These results suggest that the drop in internal damage and frost scaling of mortars was due to the beneficial effect of PCM. On one hand, it has been demonstrated elsewhere [15] that these admixtures delay the achievement of undercooling conditions and hence ice nucleation in the capillary pores. On the other hand, the mortar matrices containing PCM had different physical and mechanical properties than the reference mortar ones and therefore both their negative and positive influence on freeze/thawing resistance should be taken into account in this discussion. The reduction of effective porosity for PCM-containg mortars probably had a positive impact on increasing the frost resistance of the composite since reabsorption and redistribution of water during the thawing phase are diminished [25,45]. Also on the positive side, it has been largely discussed that a larger coefficient of thermal expansion, which is observed in PCM mortars, reduces the deformation gradient between ice and mortar matrix which results in less pore pressure during thawing and/or less scaling damage (according to the glue-spall theory [46, 47, 17]. In addition to positive changes in the mortar microstructure produced by the introduction of PCM, also properties unfavourable to frost action were caused by these admixtures. As discussed in section 3.1.2, the pore structure of PCM10 was markedly refined since the gel porosity dominated the critical mercury percolation rather than the big capillary pores. This refinement was independent on the content of inner CSH but most likely had to do with the increase of the outer CSH fraction, which is known to be inherently porous as shown in Section 3.1.1. With regards to internal damage mechanisms it has been theroetically [5] and experimentally [48] shown that finer pore structures are more susceptible to frost damage because of the increasingly large crystallization pressures encountered as the pore sizes decrease. Moreover, a higher fraction of outer CSH means that the micromechanical properties of the cementitious matrix are lowered with respect to those of the reference mortar. Consequently, microcracks might form and hence the moisture uptake during thawing is increased.

PCM30 on the other side showed the least length change and mass scaling after the first freeze/thaw cycle, which indicated that the admixtures successfully helped mitigating frost action during the cycle. But after 3 cycles this mortar presented relative length changes of one order of magnitude higher than the reference mortar while the scaled mass was the lowest among the studied mortars. The abnormally large internal damage can be attributed to the following events likely to have happened during the cycles successive to the first one. In section 3.1.2, it was shown that PCM30 presented increases of both gel and capillary porosity compared to the reference. With respect to PCM10, the gel porosity seemed to be comparable but the threshold diamater moved to the size range of capillary pores, denoting a broadening of the percolated pore sizes. The effective porosity was consequently increased with respect to PCM10 mortar. In these conditions, reabsorption of freezing solution was increased. Moreover, PCM30 presented the lowest micromechanical properties of the matrix, judging from the increase on outer CSH fraction and gel porosity and from the drop on high density CSH fraction, as well as from the X-ray attenuation drop. Both increase of reabsorption and lower micromechanical properties probably resulted on microcracking prior to (at most) the third weathering cycle. Only after 7 cycles, PCM30 overtook the other mortars and showed signs of severe scaling. From the results presented in this research, it results clear that internal damage due to frost action might have accelerated the surface scaling in PCM30 which low micromechanical properties might have aided the propagation of cracks towards the samples surface. The

fact that the same final trend was found for both internal and salt scaling damages indicates that the same risk factors steer both types of damage in mortar with PCM.

Obviously, the behavior of the studied mortars exposed to freezing/thawing cycles is bond to change if the boundary conditions are varied. It is believed by the authors that a shorter, slower, more realistic cooling may result in a substantially better performance of the PCM-containing mortars. As studied elsewhere [15], PCM can potentially smooth the temperature peaks during exposure and hence lessen the period to which the mortars are exposed to such extreme temperatures.

5. Conclusions

In this experimental investigation we studied the frost resistance of mortar with different amounts of microencapsulated PCM. The internal damage and salt scaling were assessed via standardized methods such as length change measurements and monitoring of scaled mass, but also a spatial distribution of the damage could be extracted from X-ray microtomography data. In order to explain the observed behavior, the pore system and the microstructure of the mortars were characterized through MIP and SEM analysis. Macroscopic properties of the mortars, like compressive and flexural strength and coefficient of thermal expansion, were also assessed.

The following conclusions can be drawn from the exhaustive experimental study performed herein:

- The studied microencapsulated PCM influenced cement hydration and the final microstructure of the mortar matrix as can be deduced from the increase of low density CSH volumetric fraction.
- The pore structure of the mortar matrices was modified by the inclusion of PCM admixtures. For low aggregate replacement by PCM, namely 10 % by volume of cement paste, a refinement of the pore structure occurs with an increase of gel porosity but very low capillary porosity and effective porosity. For larger replacements, like 30 %, both gel and capillary porosity are increased with respect to the reference, although the effective porosity remains lower than that of the reference mortar.
- The replacement of aggregates by the mechanically weak PCM, together with the increase of outer CSH gel volumetric fraction and of capillary and gel porosity, may have contributed to the reduction of the macroscopic compressive and flexural strength of the composites with PCM.
- For the materials and experimental conditions employed in this study, the results suggest that a limited amount of PCM in mortar may be beneficial for the frost and scaling resistance of mortar. For low replacements, namely 10 % by volume of paste, relative length changes were reasonably lower than that of reference mortar and scaling was reduced by 60 %. For higher amounts of PCM (30 % by volume of paste), the frost resistance of the mortar was lower than that of the reference mortar. In fact, the measured reduction of mechanical strength and increase in porosity were far more influential on the frost resistance of the mortar than any possible positive effect of PCM addition.
- In addition to the effect of alleged latent heat release, PCM admixtures may have increased the frost resistance of mortar by decreasing the effective porosity of the composite, specially for lower PCM replacements. It has been shown before [25], that a lower uptake of freezing medium during thawing periods, leads to decreased internal damage. Furthermore, the introduction of PCM resulted in higher coefficient of thermal expansion, which has been long associated with increased scaling resistance under the glue-spall theory [17].

Declaration of competing interest

None.

Acknowledgements

This project was carried out within the European Union's Seventh Framework Programme for research, technological development and demonstration under the ERA-NET Plus Infravation programme, grant agreement No. 31109806.0001. The authors would like to thank Encapsys, LLC, for providing the encapsulated PCMs. The first author acknowledges the financial support from the Construction Technology Research Program funded by the Ministry of Land, Infrastructure and Transport of the Korean Government under the grant 17SCIP–B103706-03. S. Chaves Figueiredo would like to acknowledge the funding from Science Without Borders from the National Council for Scientific and Technological Development of Brazil (201620/2014–6). The authors would like to acknowledge Natalie Müehleisen for the revision of the language. The contribution of Johan Bijleveld for performing DSC measurements is greatly appreciated.

References

[1] P. Mehta, P. Monteiro, Concrete: Microstructure, Properties and Materials, New York.
[2] H. Cai, X. Liu, Freeze-thaw durability of concrete: ice formation process in pores, Cement Concr. Res. 28 (9) (1998) 1281–1287.
[3] A.M. Neville, et al., Properties of Concrete, vol. 4, Longman London, 2011.
[4] T. Powers, Resistance to weathering–freezing and thawing 169, American American Society for Testing and Materials Special Report Technical Publication, 1956, pp. 182–187.
[5] G.W. Scherer, Crystallization in pores, Cement Concr. Res. 29 (8) (1999) 1347–1358.
[6] J. Newman, B.S. Choo, Advanced Concrete Technology, Elsevier, 2003.
[7] T.C. Powers, T. Willis, The air requirement of frost resistant concrete, in: Highway Research Board Proceedings, vol. 29, 1950.
[8] A. Sakulich, D. Bentz, Limiting freeze/thaw damage in cementitious infrastructure systems with phase change materials (PCMs), Microsc. Microanal. 17 (S2) (2011) 1482–1483, https://doi.org/10.1017/S1431927611008282. URL, http://www.journals.cambridge.org/abstract_S1431927611008282.
[9] A.R. Sakulich, D.P. Bentz, J. Mater. Civ. Eng. 24 (8) (2012) 1034–1042, https://doi.org/10.1061/(ASCE)MT.1943-5533.0000381. URL, http://ascelibrary.org/doi/10.1061/%28ASCE%29MT.1943-5533.0000381.
[10] B. Šavija, Smart crack control in concrete through use of phase change materials (PCMs): a review, Materials 11 (5) (2018) 654, https://doi.org/10.3390/ma11050654. URL, http://www.mdpi.com/1996-1944/11/5/654.
[11] Y. Farnam, H.S. Esmaeeli, P.D. Zavattieri, J. Haddock, J. Weiss, Incorporating phase change materials in concrete pavement to melt snow and ice, Cement Concr. Compos. 84 (2017) 134–145, https://doi.org/10.1016/j.cemconcomp.2017.09.002. URL, http://linkinghub.elsevier.com/retrieve/pii/S0958946516307417.
[12] S.Y. Kong, X. Yang, S.C. Paul, L.S. Wong, B. Šavija, et al., Thermal response of mortar panels with different forms of macro-encapsulated phase change materials: a finite element study, Energies 12 (13) (2019) 1–15.
[13] H. Cui, S.A. Memon, R. Liu, Development, mechanical properties and numerical simulation of macro encapsulated thermal energy storage concrete, Energy Build. 96 (2015) 162–174, https://doi.org/10.1016/j.enbuild.2015.03.014. URL, http://linkinghub.elsevier.com/retrieve/pii/S0378778815002066.
[14] A.M. Khudhair, M.M. Farid, A review on energy conservation in building applications with thermal storage by latent heat using phase change materials, Energy Convers. Manag. 45 (2) (2004) 263–275, https://doi.org/10.1016/S0196-8904(03)00131-6. URL, http://linkinghub.elsevier.com/retrieve/pii/S0196890403001316.
[15] J.H. Yeon, K.-K. Kim, Potential applications of phase change materials to mitigate freeze-thaw deteriorations in concrete pavement, Construct. Build. Mater. 177 (2018) 202–209, https://doi.org/10.1016/j.conbuildmat.2018.05.113. URL, https://linkinghub.elsevier.com/retrieve/pii/S0950061818311802.
[16] H.S. Esmaeeli, Y. Farnam, J.E. Haddock, P.D. Zavattieri, W.J. Weiss, Numerical analysis of the freeze-thaw performance of cementitious composites that contain phase change material (PCM), Mater. Des. 145 (2018) 74–87, https://doi.org/10.1016/j.matdes.2018.02.056. URL, http://linkinghub.elsevier.com/retrieve/pii/S0264127518301473.
[17] J.J. Valenza II, G.W. Scherer, A review of salt scaling: I. phenomenology, Cement Concr. Res. 37 (7) (2007) 1007–1021.
[18] S. Nayak, N.A. Krishnan, S. Das, Microstructure-guided numerical simulation to evaluate the influence of phase change materials (PCMs) on the freeze-thaw response of concrete pavements, Construct. Build. Mater. 201 (2019) 246–256, https://doi.org/10.1016/j.conbuildmat.2018.12.199. URL, https://linkinghub.elsevier.com/retrieve/pii/S0950061818331933.
[19] S. Pilehvar, A.M. Szczotok, J.F. Rodríguez, L. Valentini, M. Lanzón, R. Pamies, A.-L. Kjøniksen, Effect of freeze-thaw cycles on the mechanical behavior of geopolymer concrete and Portland cement concrete containing micro-encapsulated phase change materials, Construct. Build. Mater. 200 (2019) 94–103, https://doi.

org/10.1016/j.conbuildmat.2018.12.057. URL, https://linkinghub.elsevier.com/retrieve/pii/S0950061818330344.
[20] J. Kaufmann, Pore space analysis of cement-based materials by combined nitrogen sorption–wood's metal impregnation and multi-cycle mercury intrusion, Cement Concr. Compos. 32 (7) (2010) 514–522.
[21] J. Zhang, G.W. Scherer, Comparison of methods for arresting hydration of cement, Cement Concr. Res. 41 (10) (2011) 1024–1036, https://doi.org/10.1016/j.cemconres.2011.06.003. URL, http://linkinghub.elsevier.com/retrieve/pii/S0008884611001645.
[22] C.T. Rueden, J. Schindelin, M.C. Hiner, B.E. DeZonia, A.E. Walter, E.T. Arena, K.W. Eliceiri, Imagej2: imagej for the next generation of scientific image data, BMC Bioinf. 18 (1) (2017) 529.
[23] I. Arganda-Carreras, V. Kaynig, C. Rueden, K.W. Eliceiri, J. Schindelin, A. Cardona, H. Sebastian Seung, Trainable weka segmentation: a machine learning tool for microscopy pixel classification, Bioinformatics 33 (15) (2017) 2424–2426.
[24] S. Jacobsen, Scaling and Cracking in Unsealed Freeze/thaw Testing of Portland Cement and Silica Fume Concretes., Norwegian Inst. Tech., Trondheim.
[25] S. Jacobsen, D.H. Sœther, E.J. Sellevold, Frost testing of high strength concrete: frost/salt scaling at different cooling rates, Materials and structures 30 (1) (1997) 33–42.
[26] CEN/TR 15177, Testing the Freeze-Thaw Resistance of Concrete - Internal Structural Damage, Standard, CEN, Brussels, Be, 2006.
[27] K.L. Scrivener, Backscattered electron imaging of cementitious microstructures: understanding and quantification, Cement Concr. Compos. 26 (8) (2004) 935–945.
[28] T.C. Powers, T.L. Brownyard, Studies of the physical properties of hardened portland cement paste, J. Proc. 43 (1946) 101–132.
[29] X. Feng, E.J. Garboczi, D.P. Bentz, P.E. Stutzman, T.O. Mason, Estimation of the degree of hydration of blended cement pastes by a scanning electron microscope point-counting procedure, Cement Concr. Res. 34 (10) (2004) 1787–1793.
[30] M. Aguayo, S. Das, A. Maroli, N. Kabay, J.C. Mertens, S.D. Rajan, G. Sant, N. Chawla, N. Neithalath, The influence of microencapsulated phase change material (PCM) characteristics on the microstructure and strength of cementitious composites: experiments and finite element simulations, Cement Concr. Compos. 73 (2016) 29–41, https://doi.org/10.1016/j.cemconcomp.2016.06.018. URL, http://linkinghub.elsevier.com/retrieve/pii/S0958946516303110.
[31] R. Berger, J. McGregor, Effect of temperature and water-solid ratio on growth of ca (oh) 2 crystals formed during hydration of ca3sio5, J. Am. Ceram. Soc. 56 (2) (1973) 73–79.
[32] Z. Wei, G. Falzone, B. Wang, A. Thiele, G. Puerta-Falla, L. Pilon, N. Neithalath, G. Sant, The durability of cementitious composites containing microencapsulated phase change materials, Cement Concr. Compos. 81 (2017) 66–76.
[33] R.A. Cook, K.C. Hover, Mercury porosimetry of hardened cement pastes, Cement Concr. Res. 29 (6) (1999) 933–943.
[34] D. Hobbs, The dependence of the bulk modulus, young's modulus, creep, shrinkage and thermal expansion of concrete upon aggregate volume concentration, Matériaux Construct. 4 (2) (1971) 107–114.
[35] A. Jayalath, R. San Nicolas, M. Sofi, R. Shanks, T. Ngo, L. Aye, P. Mendis, Properties of cementitious mortar and concrete containing micro-encapsulated phase change materials, Construct. Build. Mater. 120 (2016) 408–417, https://doi.org/10.1016/j.conbuildmat.2016.05.116. URL, http://linkinghub.elsevier.com/retrieve/pii/S0950061816308522.
[36] X. Chen, S. Wu, J. Zhou, Influence of porosity on compressive and tensile strength of cement mortar, Construct. Build. Mater. 40 (2013) 869–874.
[37] G. Falzone, G.P. Falla, Z. Wei, M. Zhao, A. Kumar, M. Bauchy, N. Neithalath, L. Pilon, G. Sant, The influences of soft and stiff inclusions on the mechanical properties of cementitious composites, Cement Concr. Compos. 71 (2016) 153–165, https://doi.org/10.1016/j.cemconcomp.2016.05.008. URL, http://linkinghub.elsevier.com/retrieve/pii/S095894651630141X.
[38] Z. Wei, G. Falzone, B. Wang, A. Thiele, G. Puerta-Falla, L. Pilon, N. Neithalath, G. Sant, The durability of cementitious composites containing microencapsulated phase change materials, Cement Concr. Compos. 81 (2017) 66–76, https://doi.org/10.1016/j.cemconcomp.2017.04.0100958-9465/.
[39] F. Fernandes, S. Manari, M. Aguayo, K. Santos, T. Oey, Z. Wei, G. Falzone, N. Neithalath, G. Sant, On the feasibility of using phase change materials (PCMs) to mitigate thermal cracking in cementitious materials, Cement Concr. Compos. 51 (2014) 14–26, https://doi.org/10.1016/j.cemconcomp.2014.03.003. URL, http://linkinghub.elsevier.com/retrieve/pii/S0958946514000493.
[40] H. Zhang, B. Šavija, S. Chaves Figueiredo, M. Lukovic, E. Schlangen, Microscale testing and modelling of cement paste as basis for multi-scale modelling, Materials 9 (11) (2016) 907.
[41] C. Hu, Z. Li, Micromechanical investigation of portland cement paste, Construct. Build. Mater. 71 (2014) 44–52.
[42] S. Roels, K. Vandersteen, J. Carmeliet, Measuring and simulating moisture uptake in a fractured porous medium, Adv. Water Resour. 26 (3) (2003) 237–246, https://doi.org/10.1016/S0309-1708(02)00185-9. URL, http://linkinghub.elsevier.com/retrieve/pii/S0309170802001859.
[43] B. Šavija, M. Luković, E. Schlangen, J. Nanomech. Micromech. 7 (1) (2017), 04016010, https://doi.org/10.1061/(ASCE)NM.2153-5477.0000114. URL, http://ascelibrary.org/doi/10.1061/%28ASCE%29NM.2153-5477.0000114.
[44] H. Zhang, B. Šavija, M. Luković, E. Schlangen, Experimentally informed micromechanical modelling of cement paste: an approach coupling x-ray computed tomography and statistical nanoindentation, Compos. B Eng. 157 (2019) 109–122.
[45] G.W. Scherer, J. Valenza, Mechanisms of frost damage, Mater. Sci. Concr. 7 (60) (2005) 209–246.
[46] J.J. Valenza II, G.W. Scherer, A review of salt scaling: ii. mechanisms, Cement Concr. Res. 37 (7) (2007) 1022–1034.
[47] Z. Sun, G.W. Scherer, Effect of air voids on salt scaling and internal freezing, Cement Concr. Res. 40 (2) (2010) 260–270.
[48] M.D. Cohen, Y. Zhou, W.L. Dolch, Non-air-entrained high-strength concrete–is it frost resistant? Mater. J. 89 (4) (1992) 406–415.